JCI insight

RESEARCH ARTICLE

Targeting macrophage checkpoint inhibitor SIRPα for anticancer therapy

Jie Liu,[1] Seethu Xavy,[1] Shirley Mihardja,[1] Sharline Chen,[1] Kavitha Sompalli,[1] Dongdong Feng,[1] Timothy Choi,[1] Balaji Agoram,[1] Ravindra Majeti,[2,3] Irving L. Weissman,[3] and Jens-Peter Volkmer[1]

[1]Forty Seven Inc., Menlo Park, California, USA. [2]Division of Hematology, Department of Medicine, and [3]Institute for Stem Cell Biology and Regenerative Medicine, Stanford University School of Medicine, Stanford, California, USA.

The CD47/signal regulatory protein α (Cd47/SIRPα)interaction provides a macrophage immune checkpoint pathway that plays a critical role in cancer immune evasion across multiple cancers. Here, we report the engineering of a humanized anti-SIRPα monoclonal antibody (1H9) for antibody target cancer therapy. 1H9 has broad activity across a wide range of SIRPα variants. Binding of 1H9 to SIRPα blocks its interaction with CD47, thereby promoting macrophage-mediated phagocytosis of cancer cells. Preclinical studies in vitro and in vivo demonstrate that 1H9 synergizes with other therapeutic antibodies to promote phagocytosis of tumor cells and inhibit tumor growth in both syngeneic and xenograft tumor models, leading to survival benefit. Thus, 1H9 can potentially act as a universal agent to enhance therapeutic efficacy when used in combination with most tumor-targeting antibodies. We report a comparison of anti-SIRPα and anti-CD47 antibodies in CD47/SIRPα double-humanized mice and found that 1H9 exhibits a substantially reduced antigen sink effect due to the limited tissue distribution of SIRPα expression. Toxicokinetic studies in nonhuman primates show that 1H9 is well tolerated, with no treatment-related adverse effects noted. These data highlight the clinical potential of 1H9 as a pan-therapeutic with the desired properties when used in combination with tumor-targeting antibodies.

Introduction

Over the past decade, significant advances have been made in anticancer immunotherapy with the use of blocking agents against inhibitory immune checkpoints. Such immune checkpoint inhibitors work based on the premise that immune cell functions are often suppressed in cancer and relief of this suppression will improve antitumor immunity (1–3). Antibodies against inhibitory receptors expressed on T cells (such as cytotoxic T lymphocyte–associated protein 4 [CTLA-4] and programmed death 1 [PD-1]), or their ligands (such as PD-L1), have shown significant efficacy against a broad range of cancers, and clinical use is increasing. However, the increased use of these immune checkpoint inhibitor agents has led to an observation that they do not lead to clinical benefit for all patients (4–7). Many patients fail to respond or have short-lived responses, and some of them develop pronounced side effects including serious autoimmunity (8). Yet most checkpoint inhibitors that are currently approved focus on modulating T cells or the adaptive arm of the immune system.

Our previous studies have identified CD47, a cell-surface molecule, as a "marker of self" that prevents cells of the innate immune system from attacking hematologic malignancies and certain solid tumors (9–14). Targeting of the CD47/SIRPα signaling axis is emerging as a promising therapeutic intervention (15). CD47 is broadly expressed on both tumors and normal tissues, requiring higher doses of an anti-CD47–targeted therapeutic to overcome the antigen sink. Signal regulatory protein α (SIRPα) is the primary binding partner of CD47 and its cytoplasmic domain contains immunoreceptor tyrosine–based inhibition motifs, which become phosphorylated and recruit inhibitory phosphatases, in particular, Src homology 2 (SH2) domain–containing protein tyrosine phosphatases SHP-1 and SHP-2. Binding of CD47 to SIRPα triggers activation of these phosphatases and delivers a potent intracellular "don't eat me" signal to immune effector cells, such as macrophages, thereby preventing phagocytic cell activation (16–19). Unlike CD47, SIRPα has a limited tissue expression pattern, with high levels of expression observed predominantly on myeloid cells and neurons (20). Thus, relatively low doses of an anti-SIRPα agent are anticipated to be necessary to inhibit CD47/SIRPα signaling in tumors, in contrast to CD47-targeting agents, which require higher doses to effectively saturate the pathway.

Conflict of interest: ILW and RM are cofounders, equity holders, and consultants of and serve on the Board of Directors of Forty Seven Inc. JL and JV are cofounders, equity holders, and employees of Forty Seven Inc. SX, SM, SC, KS, DDF, TC, and BA are or were employees and equity holders of Forty Seven Inc.

Submitted: November 11, 2019
Accepted: May 7, 2020
Published: June 18, 2020.

Reference information: *JCI Insight*. 2020;5(12):e134728. https://doi.org/10.1172/jci.insight.134728.

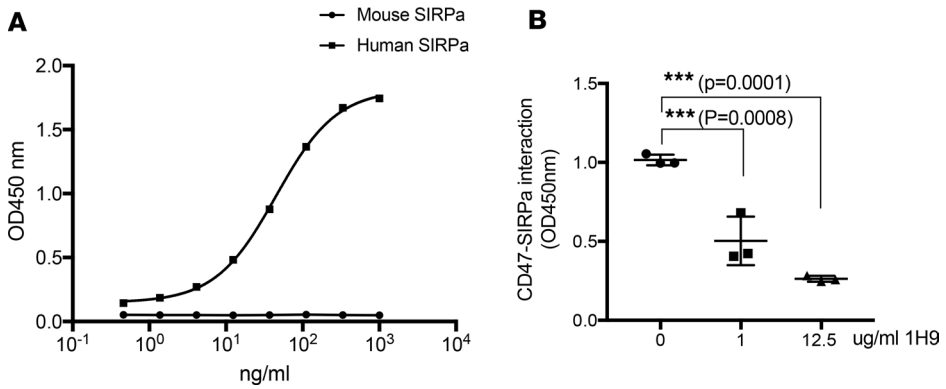

Figure 1. 1H9 binds human SIRPα specifically and blocks the binding of SIRPα to CD47. (**A**) Binding of 1H9 to human and mouse SIRPα-Fc fusion proteins was determined by ELISA. (**B**) SIRPα binding to human CD47-Fc fusion was detected by ELISA in the absence or presence of increasing concentrations of 1H9 as indicated. Each sample was assayed in triplicate. Data represent mean ± SD. The indicated *P* values were determined by multiple 1-way ANOVA.

Here we describe the development of a humanized anti-SIRPα monoclonal antibody, 1H9, and its preclinical efficacy in vitro and in vivo against various types of human tumors. 1H9 recognizes the most common allelic SIRPα variants in humans and does not bind SIRPγ, which is a close relative of SIRPα expressed on activated T cells. Since SIRPα is not present on RBCs, 1H9 does not cause a transient anemia when administered to animals and has a substantially reduced antigen sink. These findings suggest that 1H9 may provide a promising approach to deliver therapeutic benefit of CD47/SIRPα blockade for anticancer therapy when used in combination with a tumor-targeting agent.

Results

Anti-SIRPα monoclonal antibody generation and humanization. A cDNA fragment of human SIRPα encoding the extracellular domain was fused to mouse Fc to generate a SIRPα-Fc fusion protein, which was used to immunize mice to produce mouse anti-human SIRPα monoclonal antibodies. The specificity of selected hybridoma clones was examined by ELISA binding to human SIRPα-Fc. One of the positive clones, designated as 1H9, not only bound human SIRPα but also blocked the interaction of SIRPα and CD47. As expected, 1H9 did not cross-react with mouse SIRPα (Figure 1, A and B).

Humanization of 1H9 was achieved by CDR grafting onto human germline frameworks (21) and was constructed as human IgG1 with the N297A substitution to silence the Fc-dependent effector functions. To assess the antigen-binding specificity of humanized 1H9, competition binding between humanized and parental mouse 1H9 was conducted by ELISA. It showed that humanized 1H9 competed with mouse 1H9 for SIRPα binding in a dose-dependent manner (Supplemental Figure 1; supplemental material available online with this article; https://doi.org/10.1172/jci.insight.134728DS1), suggesting that humanized 1H9 possesses the same antigen-binding specificity as its parental antibody. The antigen-binding affinity of humanized 1H9 was then measured using surface plasmon resonance. Humanized 1H9 bound to a monomeric human SIRPα antigen with a K_D of 1.15×10^{-9} M, well within the range of clinically approved antibodies (Table 1 and ref. 22).

Humanized 1H9 synergizes with therapeutic antibodies to promote macrophage-mediated phagocytosis and exhibits prolonged receptor occupancy on macrophages. We next investigated the ability of humanized 1H9 to induce the phagocytosis of cancer cells by human monocytes–derived macrophages. Tumor cell lines were screened for SIRPα expression. None of the cancer cell lines used in this study expressed SIRPα. As shown in Figure 2, humanized 1H9 alone did not induce phagocytosis; however, when combined with rituximab (Rx) or cetuximab (Cx), it induced significantly higher phagocytic activity of the tumor cells than either agent alone, and the synergistic activity was observed across a range of concentrations of humanized 1H9 (Figure 2, A and B). In addition, we tested the synergy between humanized 1H9 and avelumab (Avl), an anti–PD-L1 antibody. Humanized 1H9 enhanced Avl-mediated phagocytic activity (Figure 2C). The immune checkpoint CD47/SIRPα is relevant for not only macrophages but also other SIRPα-expressing myeloid immune cells such as neutrophils. To explore if 1H9 could also mediate cancer cell cytotoxicity by neutrophils, an in vitro neutrophil cytotoxicity assay was performed. Consistent

Table 1. Binding affinity of 1H9

	K_D
1H9	2.06×10^{-9} M
Humanized 1H9	1.15×10^{-9} M

Binding of 1H9 to monomeric SIRPα was measured and analyzed by surface plasmon resonance yielding the indicated binding constants.

with a previous study (23), 1H9 did not promote cancer cell killing as a single antibody, but promoted neutrophil-mediated cytotoxicity of Raji cancer cells when combined with Rx (Supplemental Figure 2).

Taken together, our results suggested that 1H9 could act as a universal agent when used in combination to enhance the efficacy of anticancer therapeutic antibodies.

We next examined whether 1H9 treatment could result in loss of surface expression of SIRPα on macrophages and/or 1H9 internalization. Human monocytes–derived macrophage cells were incubated with 1H9 at 37°C at different time points. We found significant cell surface staining of 1H9 at all time points tested (Figure 3A), and the surface staining was detectable up to 24 hours (data not shown), as compared with the incubation done at 4°C as a control for surface staining. These data indicate that 1H9 and/or SIRPα are stable on the cell surface, which may in turn contribute to sustained in vivo therapeutic efficacy. 1H9 internalization was then further investigated during 1H9 and Rx-mediated phagocytosis of Raji cells. Strikingly, 1H9 was maintained on the cell surface of macrophages that had undergone phagocytosis, whereas Rx was internalized as rapidly as within 20 minutes (Figure 3B). Similarly, detection of surface 1H9 on phagocytosing macrophages was seen at all time points tested up to 24 hours. These results suggest that SIRPα expression was not downregulated during the phagocytosis process, which may be critical for antitumor activity when an anti-SIRPα antibody, such as 1H9, is used.

Humanized 1H9 has broad activity across various SIRPα variants. SIRPα is highly polymorphic in the IgV domain. In humans, the SIRPα protein is found in 2 major forms, V1 and V2 variants. These 2 forms of SIRPα constitute more than 80% of SIRPα present in humans (24, 25). To determine binding activity of 1H9 to different SIRPα variants, we constructed SIRPα V1 and V2 fusion proteins and tested the binding. As shown in Figure 4A, 1H9 bound both SIRPα V1 and V2, as compared with the irrelevant fusion protein.

Next we screened 22 normal human donors and genotyped their SIRPα variants. The donors were identified with V1/V1 homozygous, V2/V2 homozygous, and V1/V5 heterozygous status for SIRPα (Supplemental Table 1). Similarly, humanized 1H9 bound at comparable levels to each of V1/V1, V2/V2, and V1/V5 alleles using the donors' monocytes and macrophages (data not shown). Furthermore, we tested if 1H9 can block interaction of CD47 and SIRPα that is encoded as different variants. Monocytes were isolated from donors encoding V1/V1, V2/V2, and V1/V5 and incubated with CD47-Fc fusion protein in either the absence or presence of increasing concentrations of humanized 1H9. Humanized 1H9 blocked the interaction of CD47 and SIRPα in a dose-dependent manner, and its blocking activities were comparable among the different SIRPα variants (Figure 4B).

The most important question is whether 1H9 functions equally across these human SIRPα variants. Macrophages were then differentiated from donors encoding the different SIRPα variants. As shown in Figure 4C, humanized 1H9 synergized with Cx to promote equal levels of phagocytosis across donors with V1/V1, V2/V2, and V1/V5 variants. Taken together, our data suggest that humanized 1H9 has therapeutic potential across most patient populations.

Cross-reactivity of humanized 1H9 to the other SIRP family member. SIRPγ is a close relative of SIRPα expressed on activated T cells (26). Unlike the other SIRP family members, SIRPγ does not contain any obvious signaling domains, but binds to CD47 with a lower affinity when compared with SIRPα (26–28). SIRPγ is expressed by T cells where it interacts with CD47 on the surface of target cells, resulting in increased cell-cell adhesion in an integrin-independent manner (27). Therefore, SIRPγ may be involved in T cell responses (27). Thus, it is important to investigate the interaction of 1H9 with SIRPγ and the effects of 1H9 on T cell activation. SIRPγ His-fusion proteins were generated and binding of 1H9 to SIRPγ was tested. In the binding study, we included Kwar, which is an anti-human SIRPα antibody we previously developed and reported (23), as a control. ELISA binding showed that Kwar bound SIRPγ; however, no binding

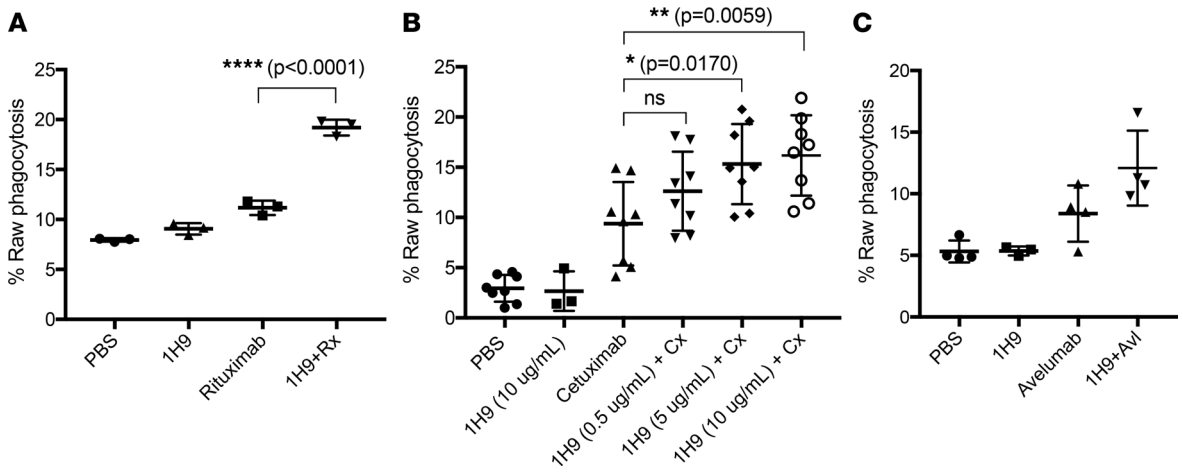

Figure 2. Humanized 1H9 synergizes with therapeutic antibodies to promote macrophage-mediated phagocytosis. (**A**) Raji (human B cell lymphoma line), (**B**) ES2 (human ovarian cancer cell line), and (**C**) HT-29 (human colorectal adenocarcinoma cell line) tumor cells were incubated with human peripheral blood–derived macrophages (n = 3–8 donors) in the presence of 10 μg/mL humanized 1H9, unless otherwise indicated, 10 μg/mL of rituximab, 10 μg/mL of avelumab, or 0.1 μg/mL of cetuximab, either alone or in combination. Two hours later, phagocytic index was determined by flow cytometer and defined as the percentage of macrophages that have phagocytosed the target cells. The indicated P values were determined by multiple 1-way ANOVA. ns, not significant. Each dot represents an individual human donor.

of 1H9 to SIRP was detected (Figure 5A). To test the efficacy of T cell proliferation blockade in vitro, we coincubated CellTrace Violet–labeled $CD4^+$ human T cells with DCs that were derived from different human allogeneic donors. Treatment with DCs promoted substantial T cell proliferation, as compared with T cells only (data not shown). Nivolumab, an anti–PD-1 therapeutic antibody, significantly enhanced T cell proliferation. As expected, 1H9 had no impact upon T cell proliferation either alone or in combination with nivolumab, confirming the lack of binding of 1H9 to SIRPγ (Figure 5B). Kwar has little effect on T cell proliferation, which is consistent with our prior experience with Kwar.

Combination treatment with humanized 1H9 inhibits tumor growth in syngeneic and xenograft mouse models. We investigated in vivo efficacy of 1H9 alone or in combination with an anti–mouse PD-L1 using a mouse melanoma syngeneic tumor model. hCD47/hSirpα Biocytogen mice engrafted with B16F10 melanoma cells were assigned to treatment with either PBS (vehicle), 1H9 (10 mg/kg), anti–mouse PD-L1 (10 mg/kg), or a combination of 1H9 and anti–mouse PD-L1. As expected, 1H9 or anti–mouse PD-L1 monotherapy showed minimal effects on tumor engraftment compared with the control. However, the combination treatment of 1H9 with the anti–mouse PD-L1 significantly reduced the tumor burden (Figure 6A). Given the aggressiveness of B16F10, treatment of 1H9 in combination with anti–mouse PD-L1 did not completely eliminate disease in any mice. However, analysis of tumor growth of the individual animals over the course of the study indicated that 1H9 in combination with anti–mouse PD-L1 slowed tumor growth compared with all the other treatment groups (Figure 6A), and animals in the combination treatment of 1H9 and anti–mouse PD-L1 survived longer compared with the other treatment groups (Figure 6B). In this study, we also treated the mice with an anti-CD47 antibody clone MIAP410 at the same dose level as 1H9 (10 mg/kg) and showed that MIAP410 was less effective than 1H9, possibly due to a larger CD47 antigen sink. As expected and previously reported for MIAP410 and other CD47 antibodies, MIAP410 induced a transient anemia (Supplemental Figure 3 and refs. 9, 11, 29). In contrast, no anemia was observed in mice treated with 1H9.

A second in vivo efficacy study was performed in the xenograft mouse model using hSirpα B-NDG Biocytogen immunodeficient mice to evaluate 1H9 in combination with Rx. Mice engrafted with GFP-luciferase–labeled Raji cells were assigned to treatment with either control PBS (vehicle), 1H9 (10 mg/kg), or Rx (10 mg/kg) or a combination of 1H9 and Rx, then followed by in vivo bioluminescent imaging to determine the level of engraftment. Compared with control, single-agent treatment with 1H9 or Rx showed no or minimal effects on tumor growth, respectively, but the combination treatment of 1H9 with Rx significantly inhibited tumor growth (Figure 6C), suggesting that 1H9 potently synergizes with Rx in the treatment of NHL-engrafted mice.

Humanized 1H9 demonstrates good safety profile and exhibits less antigen sink in vivo. Given its restricted tissue expression, direct targeting of SIRPα by 1H9 should not impact RBCs and it should have a minimal tissue antigen sink. To this end, we administered humanized 1H9 as a single dose of 5 mg/kg into

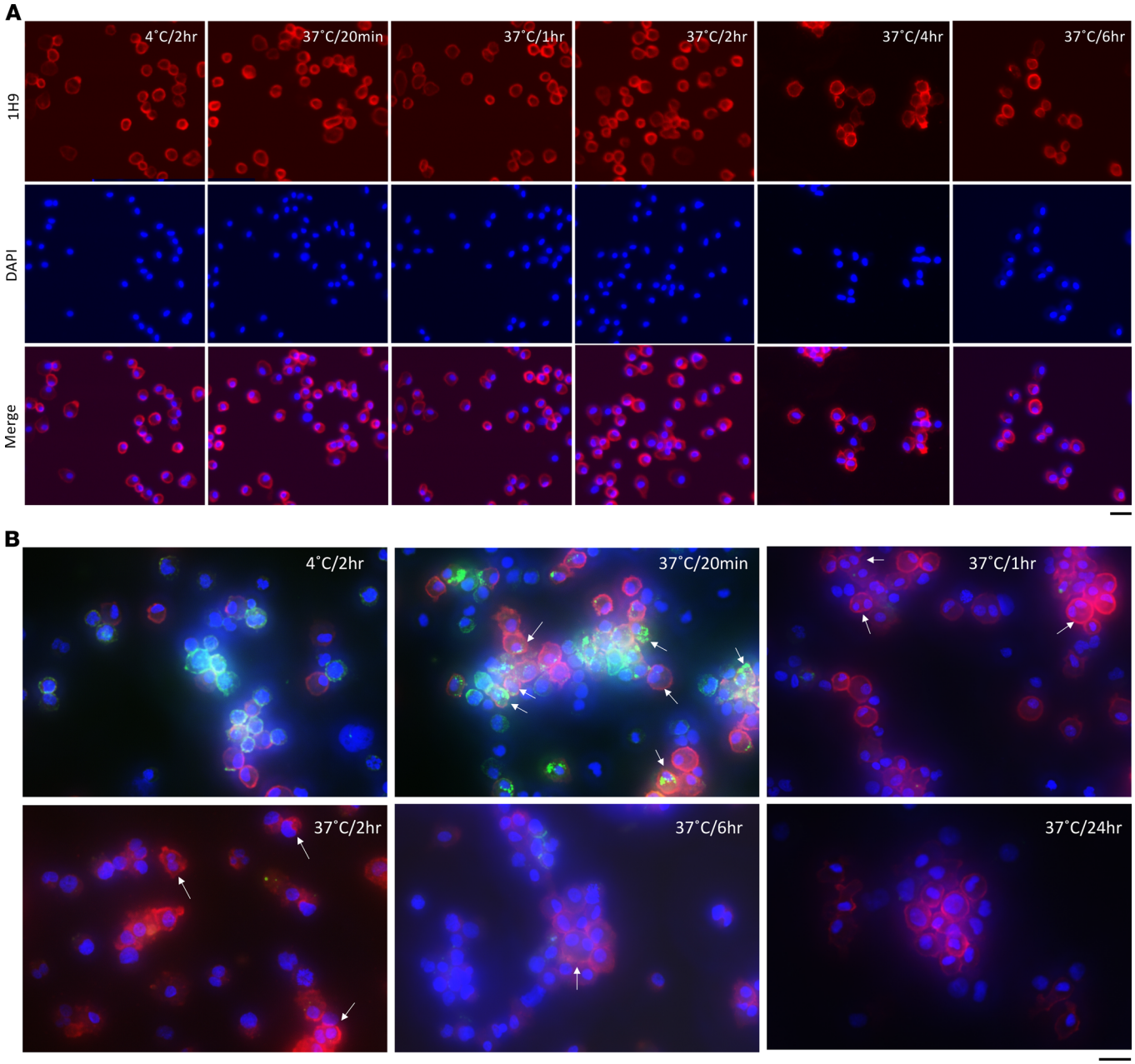

Figure 3. Internalization of humanized 1H9. (**A**) Macrophages derived from human monocytes were incubated with 10 μg/mL of humanized 1H9 at 4°C for 2 hours or at 37°C for 20 minutes, 1, 2, 4, and 6 hours. Binding of 1H9 on the cells was detected by PE-conjugated anti-human IgG1 antibody (red). Nuclei were identified by DAPI (blue). (**B**) Phagocytosis was conducted using Raji cells and human monocytes–derived macrophages in the presence of 10 μg/mL humanized 1H9 and 10 μg/mL of FITC-labeled rituximab at either 4°C for 2 hours or 37°C for 20 minutes, 1, 2, 6, and 24 hours. Red: 1H9, Green: rituximab, Blue: nuclei. Arrows indicate phagocytosed cells. Scale bars: 20 μm.

CD47/SIRPα double-humanized mice. No RBC loss or anemia was observed (Figure 7A). However, consistent with our previous report (11), 5F9 induced transient anemia on day 3, and in all animals, the hemoglobin decrease spontaneously resolved, returning to baseline levels after 2 weeks (Figure 7A). In addition, we compared 1H9 and 5F9 for their receptor occupancies (RO) on monocytes in CD47/SIRPα double-humanized mice. 1H9 at a single dose of 5 mg/kg achieved 100% RO at 4 hours after administration. The maximal RO was sustained for at least 4 days (Figure 7B). Due to a larger sink effect, administration of 5 mg/kg 5F9 achieved maximal RO, ranging from 13% to 76%, and the RO decreased on day 2 (Figure 7C). It is anticipated that a higher dose of 5F9 can achieve the similar RO as 1H9 in this animal model by overcoming the larger sink.

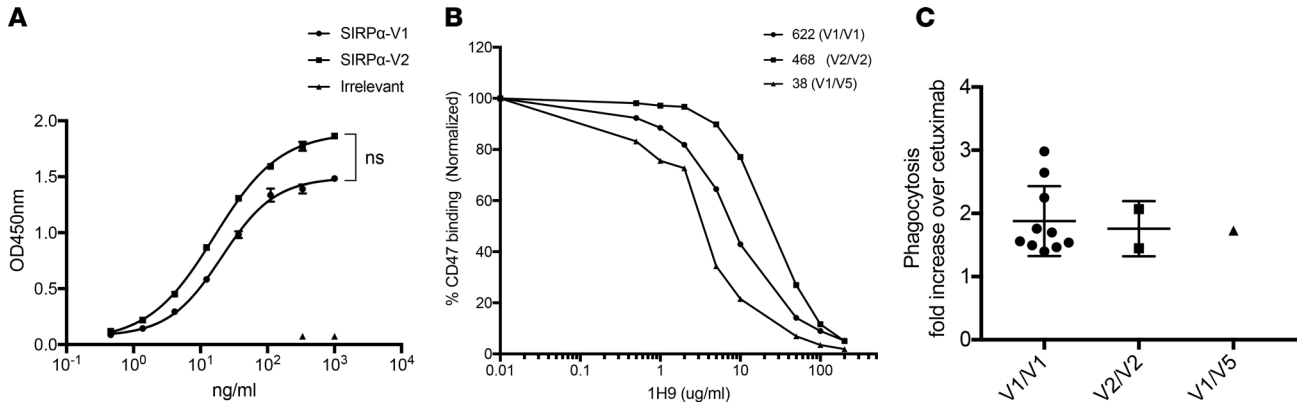

Figure 4. Humanized 1H9 binds to different SIRPα variants and synergizes with cetuximab to promote phagocytosis across donors expressing different SIRPα variants. (**A**) ELISA binding of 1H9 to human SIRPα-V1, SIRPα-V2, and an irrelevant Fc fusion proteins under increasing concentrations as indicated. Each sample was assayed in triplicate. Data represent mean ± SD. (**B**) Monocytes derived from 3 human donors, which express SIRPα as V1/V1, V2/V2, and V1/V5 variants, were incubated with 1 μg/mL AF488-labeled CD47-Fc fusion protein in the absence or presence of increasing concentrations of humanized 1H9. Binding of CD47 on the cells was measured and analyzed by flow cytometry. Binding was calculated and normalized on the mean fluorescence intensity of CD47/SIRPα binding in the absence of 1H9 as 100%. (**C**) HT-29 tumor cells were labeled with CFSE and incubated with human monocyte–derived macrophages, which express SIRPα as V1/V1 (n = 10), V2/V2 (n = 2), and V1/V5 (n = 1) variants, in the presence of 10 μg/mL humanized 1H9 or 0.1 μg/mL cetuximab, either alone or in combination. Fold increase of phagocytosis was calculated by phagocytosis induced by the combination treatment over phagocytosis induced by cetuximab alone.

To study the pharmacokinetic and toxicology profile, the cynomolgus monkey was selected. Human and cynomolgus monkey have a high degree of amino acid sequence identity for SIRPα (92.8%), whereas the sequence identity between human and mouse (66.1%) or rat SIRPα (66.5%) is very low. 1H9 does bind cynomolgus but not mouse SIRPα. The affinity of 1H9 to monkey SIRPα was determined to be approximately 2 nM. A 4-week non-GLP repeat-dose toxicology study was conducted in female cynomolgus monkeys. Administration of 1H9 by i.v. infusion was well tolerated in all monkeys at all dose levels tested (10, 30, or 100 mg/kg/dose). There were no abnormal clinical observations or 1H9-related effects on body weight or food consumption at doses up to 100 mg/kg/dose. There were no 1H9-related changes for clinical chemistry or hematology. No transient anemia was observed with 1H9 infusion when compared with vehicle control group (Figure 8A). In addition, there were no 1H9-related changes in gross pathology, mean study group organ weights, or microscopic findings. In summary all doses were well tolerated.

Plasma exposures of 1H9 were measured and analyzed. After 4 weekly i.v. infusions of 1H9 at doses of 10, 30, and 100 mg/kg, approximately dose-proportional increases in C_{max} and AUC were observed on days 1, 8, 15, and 22 over the dose range 10 to 100 mg/kg. Some accumulation in 1H9 exposure was observed after once-weekly i.v. administration over 4 weeks, with mean accumulation ratios for serum concentration at the end of the dosing interval of 168 hours (C_{trough}) ranging from 1.6 to 2.1; accumulation ratios for C_{max} ranging from 1.2 to 1.6; and accumulation ratios for $AUC_{0\text{-}168h}$ ranging from 1.4 to 1.9 (Figure 8B).

Discussion

Accumulating evidence suggests that blockade of the CD47/SIRPα immune checkpoint pathway is a promising new way to treat human cancer. This led to the development of various CD47/SIRPα–blocking agents, and these agents have shown efficacy in vitro and in preclinical studies against various types of human tumors. A number of these agents are now being tested in phase 1/2 clinical trials, including the humanized 5F9 monoclonal antibody developed in our lab, which has shown efficacy in diffuse large B cell lymphoma, follicular lymphoma, acute myeloid leukemia, and myelodysplastic syndromes (11, 15, 29). These promising results prompted us to develop antibodies against SIRPα, the cognate receptor for CD47 on macrophages.

Analysis of the distribution and frequency of SIRPα polymorphisms across diverse human populations indicates that SIRPα is highly polymorphic, and thus the development of widely effective SIRPα antagonists is challenging. Among the different SIRPα allelic variants, V1 and V2 are the predominant variants among diverse populations (24, 25). Humanized 1H9 recognizes both V1 and V2 variants with

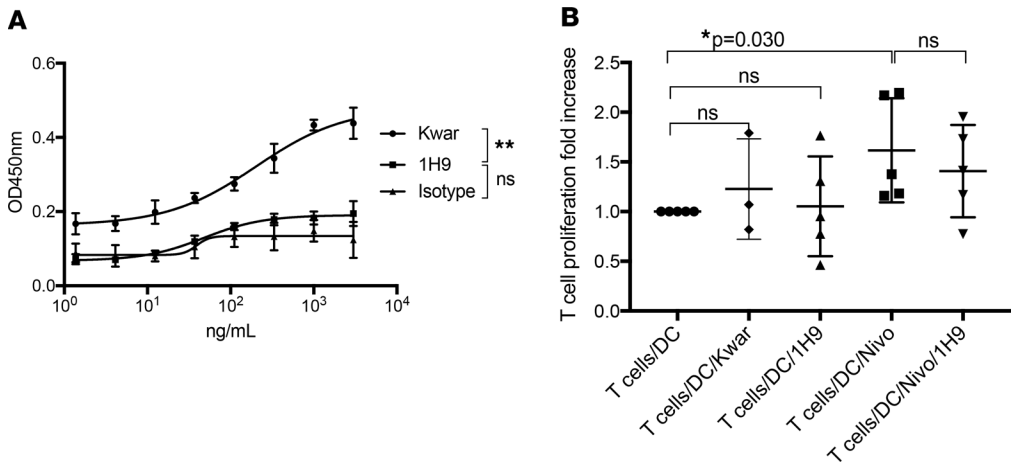

Figure 5. Cross-reactivity of humanized 1H9 to SIRPγ. (**A**) Binding of anti-SIRPα antibodies 1H9 and Kwar to human SIRPγ was determined by ELISA under increasing concentrations as indicated. Data represent mean ± SD. Each sample was assayed in duplicate (***P* value = 0.004). (**B**) Human T cells from 2 donors and monocyte-derived DCs differentiated from 5 different human allogeneic donors were cocultured at 5:1 ratio in the presence of 10 μg/mL of 1H9, Kwar, nivolumab, or a combination. Proliferated T cells were gated on divided CellTrace Violet^{low} CD4$^+$ T cells and the fold change in proliferation over T cells and DCs without the addition of an antibody was presented. The indicated *P* values were determined by multiple 1-way ANOVA. ns, not significant. **P* value = 0.030.

high affinity and synergizes with Cx to enhance phagocytosis, using macrophages derived from human donors, which encode V1/V1, V2/V2, and V1/V5 alleles (Figure 4, A–C). Thus, our data suggest 1H9 has the potential to be effective in a broad range of patients.

1H9 does not opsonize tumor cells directly and its efficacy both in vitro and in vivo is dependent on combing with tumor-opsonizing antibodies, possibly because 1H9 only targets the CD47/SIRPα axis on the side of the immune cells (Figures 2 And 6). Antibodies against cell surface antigens may be internalized through specific interactions with their antigens. The efficacy of certain antibody-based therapies, such as antibody drug conjugates, depends on not only binding affinity and specificity to the antigen but also internalization (30–33). In contrast, rapid internalization may not be desirable if effector functions, such as antibody-dependent cell-mediated cytotoxicity, antibody-dependent cellular phagocytosis, or complement-dependent cytotoxicity, are critical for antitumor activity. Antibody internalization can have an opposite effect because internalization can lead to rapid clearance of the drug in vivo and hence may require higher antibody doses or more frequent dosing (34–36). We showed here that 1H9 does not internalize and that SIRPα expression is not downregulated on macrophages during the process of phagocytosis (Figure 3). These features may enable prolonged receptor occupancy and sustained pharmacologic action to achieve optimal efficacy. Together with the evidence of a smaller antigen sink for 1H9 (discussed below), it suggests that 1H9 should remain in its therapeutic site and less frequent dosing may be required. Development of an ideal CD47/SIRPα–blocking reagent should include careful consideration of these pharmacokinetic data.

Some anti-SIRPα antibodies may cross-react with other SIRP family members and alter their functions. SIRP, the third member of the human SIRP family, is expressed on T cells and activated NK cells. It can bind CD47, albeit with 10-fold lower affinity as compared with SIRPα. Moreover, SIRPγ-CD47 interaction mediates cell-cell adhesion and supports APC–T cell contact, enhancing antigen presentation, the consequent T cell proliferation, and cytokine secretion. It is unlikely that SIRPγ itself generates intracellular signals because it does not have any known signaling motifs. However, its role is not definitively established (26–28, 37). 1H9 does not bind SIRPγ and does not inhibit T cell proliferation in allogeneic mature DCs mixed lymphocyte reactions (Figure 5, A and B), indicating that 1H9 has no effect on APC-mediated T cell function.

SIRPα expression is mainly restricted to myeloid cells and neurons, potentially enabling a lower effective dose and improving pharmacokinetics and/or pharmacodynamics. Systemically administered CD47-blocking antibodies currently in clinical trials bind CD47 on RBCs (25,000 copies/cell) (16); however, with 5F9 that we developed (currently in multiple clinical trials), we have successfully mitigated anemia by a priming and maintenance dose strategy (11, 15, 29) and have not observed any significantly recurrent adverse events of thrombocytopenia, thrombosis, or hypertension. In this study, we demonstrated that administration of

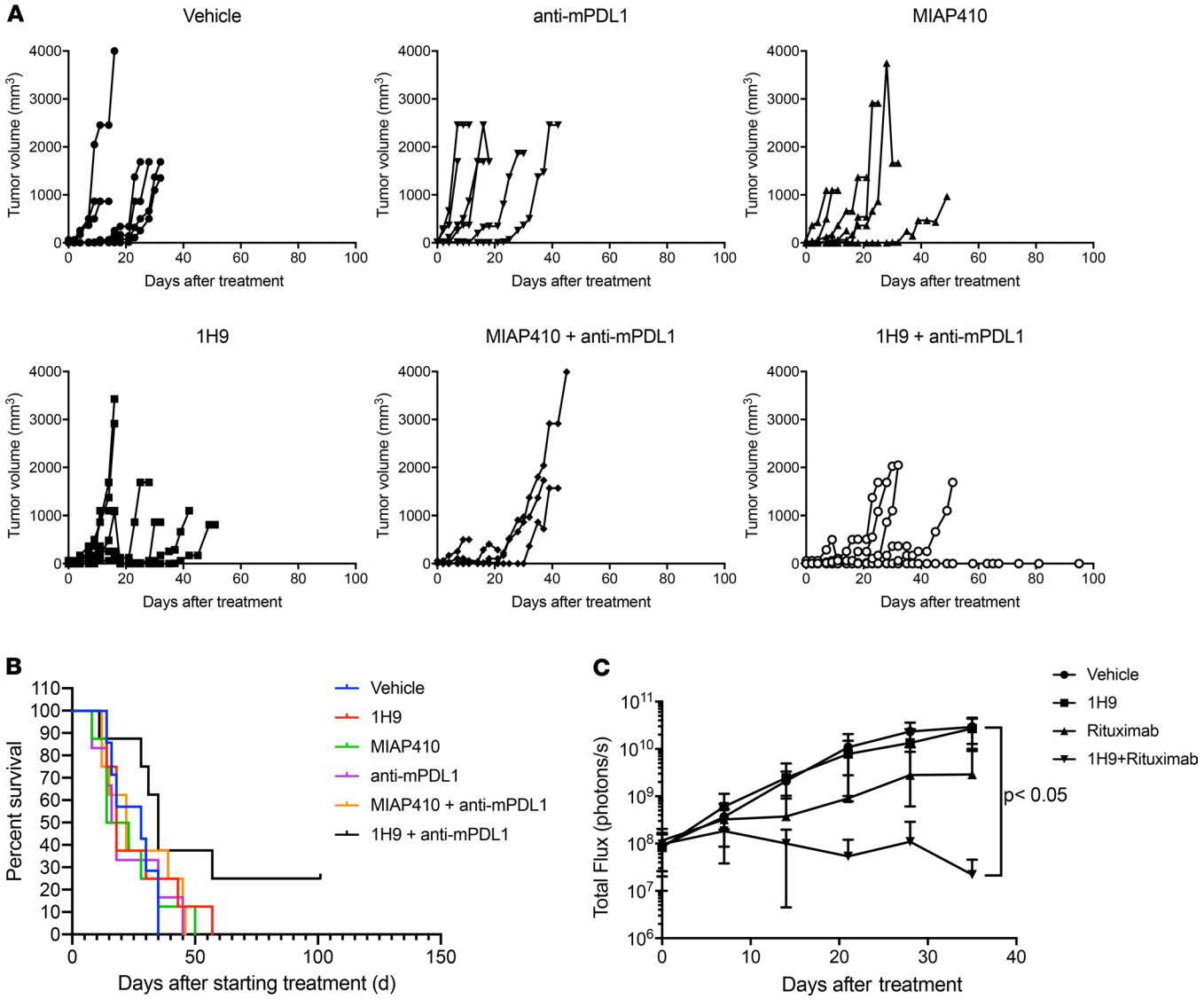

Figure 6. In vivo therapeutic activity of combination treatment with humanized 1H9. (**A**) B16F10 (2.5e5) cells were engrafted subcutaneously into CD47/SIRPα double-humanized mice (n = 7 for PBS, 6 for anti–PD-L1, and 8 for the 1H9 and MIAP410 alone and in the combination groups). Twelve days after engraftment, treatment was initiated with PBS, 10 mg/kg of 1H9, anti–PD-L1 antibody, or MIAP410, or a combination of 1H9 and anti–PD-L1 antibody 3 times a week until the termination of the study. Caliper measurements were obtained 3 times per week during treatment and until the termination of the study to assess tumor burden and/or tumor recurrence. (**B**) Kaplan-Meier plot of overall survival of B16F10-engrafted cohorts. (**C**) Raji cells were engrafted subcutaneously into SIRPα-humanized immunodeficient mice (n = 5 for each group). Ten days after engraftment, treatment was initiated with PBS, 10 mg/kg of 1H9, or rituximab, or a combination of 1H9 and rituximab 3 times a week until the termination of the study. Total flux measurements were obtained once per week during treatment and until the termination of the study to assess tumor burden and/or tumor recurrence. Statistics: repeated 1-way ANOVA with Holm-Šidák correction.

1H9 is well tolerated in both SIRPα-humanized mice (Figure 7 and Supplemental Figure 3) and nonhuman primates at multiple doses (Figure 8); no anemia or any adverse events were observed. Thus, SIRPα-targeting agents are anticipated to have an acceptable safety profile without the need for a priming dose.

Taking advantage of CD47 and SIRPα double-humanized mice, we directly compared the antigen sink of 1H9 to that of 5F9. We showed that a single 5-mg/kg dose of 1H9 is sufficient to achieve 100% receptor occupancy on monocytes, whereas only 50% receptor occupancy was observed for 5F9 at the same dose (Figure 7, B and C). Based on the narrow tissue distribution of SIRPα, we expected 1H9 would bind a smaller number of normal cells and thus require fewer molecules to achieve receptor saturation compared with anti-CD47 antibodies.

Although humanized 5F9 has demonstrated clinical response when used as monotherapy and in combination with other agents, the large sink requires an increased dose. The anti-SIRPα 1H9 can overcome the sink

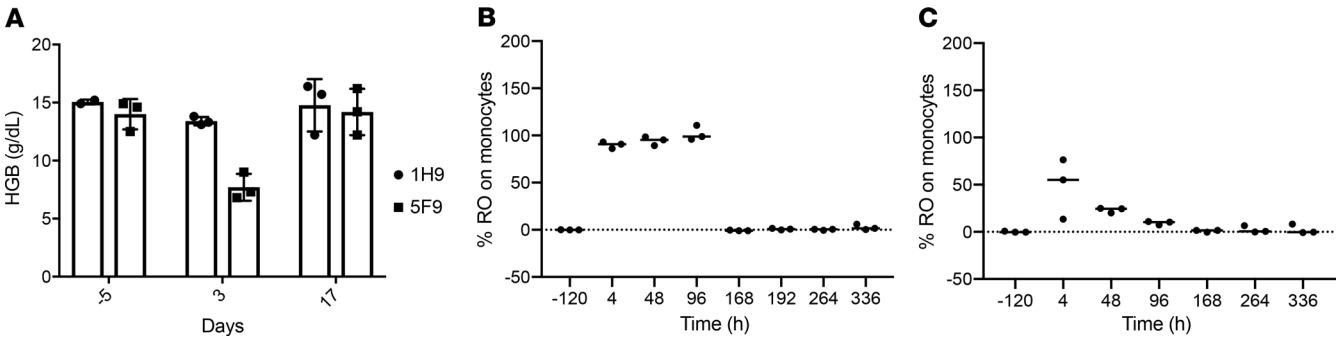

Figure 7. Humanized 1H9 does not cause anemia and exhibits a smaller antigen sink when administered in CD47/SIRPα double-humanized mice in vivo. (**A**) A single 5 mg/kg dose of 1H9 or 5F9 was given i.p. in CD47/SIRPα double-humanized mice (n = 3 for each group). Hemoglobin was measured on day 5 predose and days 3 and 17 after dose. (**B**) SIRPα and (**C**) CD47 receptor occupancies were measured on monocytes at indicated time points from CD47/SIRPα double-humanized mice treated as described in **A**.

effect, thus requiring less absolute drug to be administered, but the absence of a monotherapy effect must be considered. Since SIRPα is not present on RBCs, transient anemia is avoided by anti-SIRPα agents. We generated a humanized anti-SIRPα antibody, 1H9, and described herein the preclinical assessments of 1H9. 1H9 binds with high affinity to the most common allelic SIRPα variants in humans, blocks the CD47/SIRPα interaction, and synergizes with therapeutic antibodies to promote phagocytosis of tumor cells in vitro and inhibit tumor growth in vivo. We demonstrated that 1H9 can be safely administered to animals and has a reduced antigen sink. These findings establish 1H9 as a promising agent to further evaluate for therapeutic benefit of CD47/SIRPα blockade. Our data provide the preclinical rationale for the development of 1H9 as a promising therapeutic for oncology indications when used in combination with most tumor-targeting antibodies.

Methods

Antibody development and humanization. Anti-human SIRPα antibodies were developed by standard hybridoma technology. Hybridomas were selected and supernatants from the resulting clones were screened by ELISA and FACS. One of the hybridoma clones, termed 1H9, was cloned and sequenced. Humanization of 1H9 was performed by CDR grafting onto human germline frameworks (21).

Cell transfection. 293F cells were cultured under FreeStyle 293 Expression Medium (Invitrogen). Transient transfection was performed by cotransfection of expression vectors encoding antibody heavy

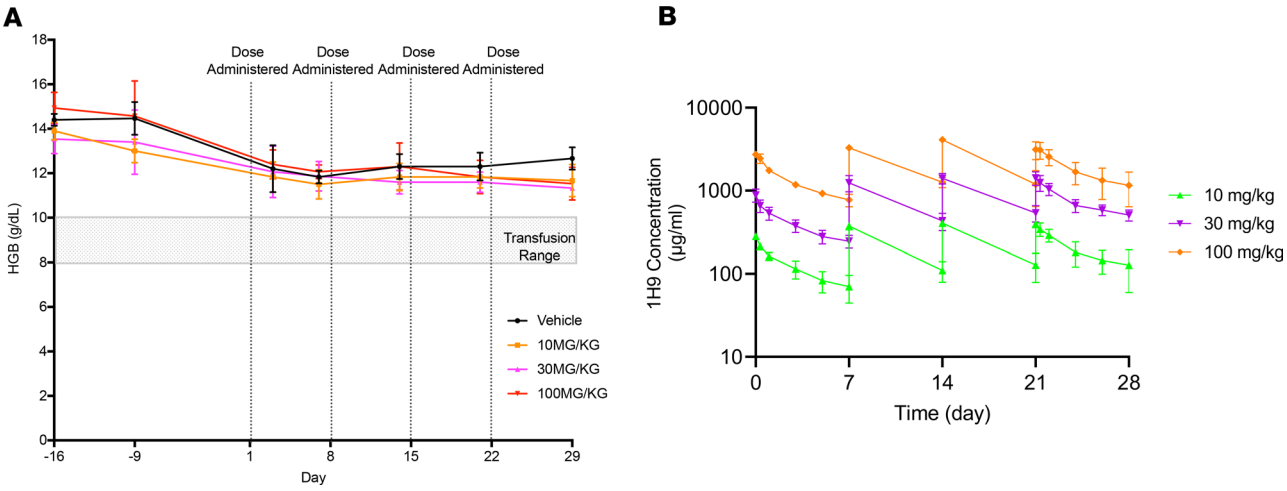

Figure 8. Nonhuman primate pharmacokinetic and toxicology studies show no adverse events associated with humanized 1H9. Humanized 1H9 was administered to cynomolgus monkeys as a single intravenous infusion at 10, 30, and 100 mg/kg (n = 3 for each group) once weekly for total of 4 weeks. (**A**) Peripheral blood was collected for hematology twice during the predose phase; on days 3, 7, 14, and 21 of the dosing phase; and on the day of scheduled sacrifice. (**B**) Serum concentration-time profiles of 1H9 after intravenous repeat doses in cynomolgus monkeys by dose group from days 1 to 28 (semilogatithmic). Values are presented as mean ± SD.

chain and light chain using 293fectin Transfection Reagent (Invitrogen), according to the manufacturer's instructions. Four to 5 days later, supernatants from the transfected cells were harvested and tested for antibody secretion by ELISA. Briefly, 96-well Nunc plates (Thermo Scientific) were coated with 1 μg/mL goat anti–human Fc γ antibody in PBS for 16 hours at 4°C. After blocking for 1 hour with 0.4% BSA in PBS at room temperature, isolated supernatants were added in 1/3 sequential dilutions and incubated for 1 hour at room temperature. Plates were subsequently washed 3 times and incubated with HRP-conjugated–goat anti–human κ-specific antibody for 1 hour at room temperature. After washing, plates were developed with TMB (Sera Care). The reaction was stopped with 2 M H_2SO_4, and OD was measured at 450 nM.

Antibody purification and characterization. The culture supernatant was applied to Protein A Sepharose columns (GE Healthcare). The column was washed with PBS, and protein was then eluted with eluting buffer (0.1 M sodium citrate buffer, pH 3.0). Collected fractions were neutralized with 1 M Tris pH 9.0. Finally, purified samples were dialyzed against PBS. Purity of the eluted antibody fraction was analyzed by SDS-PAGE on gels under reducing or nonreducing conditions. Bands were visualized by Coomassie Brilliant Blue staining.

Antibody affinity measurement. Human SIRPα-His fusion protein was made by fusing the extracellular domain of human SIRPα to His-tag and used for measuring monomeric binding affinity to 1H9. Binding experiments were performed on a Biacore 3000 at 25°C. Goat anti–human capture antibody was immobilized (as indicated in the table) on the surface of the chip by direct immobilization using EDC/NHS coupling chemistry on flow cells 2, 3, and 4 of the CM5 chip. The unoccupied sites were blocked with 1 M ethanolamine. Flow cell 1 was untreated and used as reference for subtraction of any nonspecific binding of the Ag to the chip surface. The test Abs were captured on flow cells 2, 3, and 4 at an RU as indicated. Antigen was flowed over the chip at single analyte concentration. Binding of antigen to the ligand was monitored in real-time to obtain on (ka) and off (kd) rates. The equilibrium constant (K_D) was calculated from the observed ka and kd. For the fast off-rate interactions, K_D was determined by steady state kinetic analysis. Full kinetic analysis was performed using analyte concentrations from 50 nM to 0 (if the saturating amount was 50 nM, then the analysis was performed using analyte concentrations of 50 nM and run serial dilutions to 25, 12.5, 6.25, 3.125, 1.56, and 0 or as indicated). Chi-square (χ^2) analysis was carried out between the actual sensorgram and the sensorgram generated from the BIAnalysis software to determine the accuracy of the analysis. χ^2 Value within 1–2 is considered significant (accurate) and below 1 is highly significant (highly accurate).

In vitro phagocytosis assay. Raji (ATCC CCL-86), HT29 (ATCC HTB-38), and ES2 (ATCC CRL-1978) cancer cells were washed and counted, then labeled with calcein AM at 37°C for 10 minutes. About 25 μL containing 1×10^5 calcein AM–labeled cells in serum-free IMDM were added to each well. Antibody treatment (in 25 μL) with a final concentration of 10 μg/mL of 1H9, Rx (Myoderm), Avl (Myoderm) or 0.1 μg/mL of Cx (Myoderm) was added to the wells and incubated at 37°C for 30 minutes. At 30 minutes, human monocyte–derived macrophages that had previously been harvested with TrypLE were counted and plated with 5×10^4 cells in 50 μL of serum-free IMDM. Plates were incubated at 37°C for 2 hours (effector/target = 1:2). At the end of incubation, the plate was centrifuged and the supernatant was discarded. The cells were then resuspended in 50 μL of PBS plus 2% FBS plus 5 μg/mL Alexa Fluor 647 anti-human CD206 (BioLegend, catalog 321116) and incubated on ice in dark for 30 minutes. The phagocytic index was determined by flow cytometer and defined as the percentage of macrophages that have phagocytosed the target cells.

In vitro cytotoxicity assay. About 2.5×10^5 human neutrophils isolated via the EasySep Direct Human Neutrophil Isolation Kit (Stem Cell Technologies) were cocultured with 5×10^3 CFSE-stained (Invitrogen) Raji cancer cells (ATCC CCL-86) for 4 hours in RPMI 1640 (Gibco) and supplemented with 10% human serum (GeminiBio), 10 ng/mL recombinant human G-CSF (R&D Systems), and 50 ng/mL recombinant human IFN-γ (R&D Systems). The cells were washed and stained with anti-human CD16, CD66a/c/e antibodies (BioLegend), and DAPI and analyzed by a Beckman Coulter CytoFLEX flow cytometer. The percent relative cytotoxicity of $CFSE^+$ cells was determined using FlowJo software.

Genotyping SIRPα variants. Genomic DNA was isolated from human donor blood samples using QIAamp DNA Isolation Kit (QIAGEN). PCR was performed by using the isolated genomic DNA and primers of TAGAATACAGGCTCATGTTGCAGGT and GCCTTCAGCAAATAGCATGACGT. PCR fragments were purified and sequenced. Different SIRPα variants were analyzed and identified according to SIRPα reference sequences (24).

Blocking human CD47 binding on monocytes isolated from human donors. Human PBMCs were isolated from human blood using Ficoll. Cells (5×10^5) were incubated with 1 μg/mL of AF488-conjugated human CD47-Fc fusion protein in the absence or presence of increasing concentrations of humanized 1H9. Binding of CD47 on the cells was measured and analyzed by flow cytometry.

Internalization of 1H9. Internalization of humanized 1H9 was tested by incubating 10 μg/mL of the antibody with macrophage cells differentiated from normal human monocytes at 37°C for 20 minutes, 1, 2, 4, 6, and 24 hours. Cells were then fixed and permeabilized. PE-labeled anti–human IgG1 antibody was used to detect 1H9. DAPI was used to stain nuclei. Incubation at 4°C for 2 hours was used as a control for the surface staining of 1H9.

Mixed lymphocyte reaction. Healthy monocytes were isolated from buffy coat according to the Stem Cells isolation kit. Monocyte-derived mature DCs were obtained using R&D Systems kit. On day 10, fresh human pan-T cells from a different healthy donor were isolation using Miltenyi Biotec kit. Before the mixed lymphocyte reaction assay, pan-T cells were labeled with CellTrace violet from Thermo Fisher according to the manufacturer's instruction. Harvested differentiated mature DCs were cocultured with CellTrace-labeled pan-T cells at 1:5 ratio in the presence of 10 μg/mL antibody of 1H9 or nivolumab in assay media (RPMI plus 10% FBS). Plates were incubated for 6 days at 37°C with changing of media on day 3 by removing half of the media with fresh assay media. On day 13, T cells were harvested and stained with anti-CD4 and live/dead stain for 20 minutes on ice before reading on CytoFlex instrument. Proliferated T cells were gated for live $CD4^+$ cells. Percentages of proliferated T cells were determined based on CellTace $violet^{low}$ cells. Nivolumab was obtained from Selleckchem.

Mice. Female hCD47/hSirpα C57BL/6 mice and female hSirpα B-NDG mice were purchased from Biocytogen. Studies were initiated when the mice were 8–12 weeks old.

In vivo syngeneic mouse model. About 250,000 B16F10 cells were subcutaneously engrafted in the left flank per mouse using 6- to 8-week-old female hCD47/hSirpα Biocytogen mice (Biocytogen). Treatment was initiated 10 days after engraftment when tumors were palpable. Animals were randomized based on complete blood count (CBC), body weight, and tumor volume. Mice were injected i.p. with PBS, anti-mouse PD-L1 (10 mg/kg, Bio X Cell, clone, 10F.9G2), humanized 1H9 (10 mg/kg), MIAP410 (10 mg/kg), or a combination 3 times per week until the termination of the study. The tumor volume was determined via caliper measurement and calculated using the following equation (reference): tumor volume (mm^3) = (length × $width^2$)/2. CBC was assessed before treatment and once per week after treatment was initiated. Caliper measurements were obtained before treatment and 3 times per week after treatment was initiated.

In vivo xenograft mouse model. Raji (GFP/Luciferase) were resuspended in PBS and 1×10^6 cells were engrafted subcutaneously into the left flank of each mouse. hSirpα B-NDG Biocytogen mice were used. Around 7 days after engraftment, weight measurements were obtained to determine stock concentrations for the therapeutics. Bioluminescent imaging was performed on days 2, 7, 9, and 10 after engraftment to monitor tumor size and growth. Animals were randomized based on tumor size as measured by bioluminescent imaging on days 9 and 10 after engraftment and placed into 4 cohorts with 5 animals/group. Treatment was initiated when bioluminescent imaging confirmed tumor growth — i.e., total flux was at least 2 to 3 times higher than baseline (approximated by bioluminescent imaging taken 5–7 days after engraftment). To monitor animal health, observations were made based on animal activity and general appearance. Total flux measurements were obtained once a week until the termination of the study to assess tumor burden and/or tumor recurrence.

Toxicity study in nonhuman primates. Monkeys were administered a single dose of vehicle or humanized 1H9 at 10, 30, and 100 mg/kg by a 1-hour i.v. infusion once weekly over 4 weeks (total of 4 doses). Data on clinical observations, body weight, and food consumption were collected throughout the study. Peripheral blood was collected for hematology twice during the predose phase; on days 3, 7, 14, and 21 of the dosing phase; and on the day of scheduled sacrifice. Blood samples for toxicokinetic (TK) analysis were taken at predose, 0.25, 8, 24, 72, 120, and 168 hours after the end of the infusion on days 1 and 22. In addition, blood samples were collected on days 8 and 15 predose and 0.25 hours after the end of the infusion. Serum was analyzed for 1H9 using a qualified immunoassay with a lower limit of quantification of 50.0 ng/mL. TK parameters were estimated by the noncompartmental approach using Phoenix WinNonlin 8.0. Values below the limit of quantitation before C_{max} were set to zero for analysis purposes.

SIRPα receptor occupancy assay. CD47/SIRPα double-humanized mice purchased from Biocytogen were given a single dose i.p. of 1H9 or 5F9 at 5 mg/kg. Peripheral blood was collected via the tail vein before treatment and at various time points after treatment for CBC and RO assessment. RO was determined using

a flow-based assay. A drop of blood was diluted with PBS plus 2 mM EDTA. The sample was separated into 2 aliquots, where one aliquot was incubated with 200 μg/mL of 1H9 or 5F9 for measuring the maximum occupancy and the other with FACS buffer (PBS plus 2% FBS plus 2 mM EDTA), followed by incubation with Alexa-488 anti-human IgG (Invitrogen, A-11013) and APC-anti-mouse CD45 (1:100, BioLegend). MFI was determined for monocytes and theoretical RO was calculated using the following equation: theoretical RO (%) = 100 × [(MFI test – MFI background) / (MFI max – MFI background)].

Statistics. Statistical analysis was performed using GraphPad Prism 7.0. A 2-tailed *t* test was used for comparisons between 2 groups and 1-way repeated ANOVA with Holm-Šidák correction was used for comparisons of more than 2 groups. A *P* value less than or equal to 0.05 was considered significant.

Study approval. All animal studies were reviewed by, approved by, and performed in compliance with Forty Seven Inc.'s Institutional Animal Care and Use Committee protocols. All nonhuman primate experiments were conducted in accordance with the applicable Covance Laboratories Inc. standard operating procedures, which approved these studies. All procedures in the protocol were in compliance with the Animal Welfare Act Regulations (9 CFR 3).

Author contributions

JL, RM, ILW, and JPV conceptualized the work. JL, SX, and SC are responsible for the methodology. JL, SX, SM, SC, KS, DF, BA, and TC performed experiments and analyzed data. JL wrote the original draft of the manuscript. SM, SC, RM, ILW, and JPV contributed to reviewing and editing the manuscript.

Acknowledgments

We thank Ofelia Mata and Caiaphas Ardoin for animal care and Terry Storm for lab management. We thank Kyle Elrod, Mark McCamish, Chris Takimoto, and Craig Gibbs for critical review of the manuscript.

Address correspondence to: Jie Liu, Forty Seven Inc., 1490 O'Brien Drive, Suite A, Menlo Park, California 94025, USA. Phone: 650.352.4152; Email: jliu@fortyseveninc.com or jliu6@stanford.edu.

1. Topalian SL, Taube JM, Anders RA, Pardoll DM. Mechanism-driven biomarkers to guide immune checkpoint blockade in cancer therapy. *Nat Rev Cancer*. 2016;16(5):275–287.
2. Sharpe AH. Introduction to checkpoint inhibitors and cancer immunotherapy. *Immunol Rev*. 2017;276(1):5–8.
3. Lee L, Gupta M, Sahasranaman S. Immune Checkpoint inhibitors: An introduction to the next-generation cancer immunotherapy. *J Clin Pharmacol*. 2016;56(2):157–169.
4. Tarhini A. Immune-mediated adverse events associated with ipilimumab ctla-4 blockade therapy: the underlying mechanisms and clinical management. *Scientifica (Cairo)*. 2013;2013:857519.
5. Seidel JA, Otsuka A, Kabashima K. Anti-PD-1 and anti-CTLA-4 therapies in cancer: mechanisms of action, efficacy, and limitations. *Front Oncol*. 2018;8:86.
6. Rotte A, Jin JY, Lemaire V. Mechanistic overview of immune checkpoints to support the rational design of their combinations in cancer immunotherapy. *Ann Oncol*. 2018;29(1):71–83.
7. Michot JM, et al. Immune-related adverse events with immune checkpoint blockade: a comprehensive review. *Eur J Cancer*. 2016;54:139–148.
8. Boutros C, et al. Safety profiles of anti-CTLA-4 and anti-PD-1 antibodies alone and in combination. *Nat Rev Clin Oncol*. 2016;13(8):473–486.
9. Willingham SB, et al. The CD47-signal regulatory protein alpha (SIRPa) interaction is a therapeutic target for human solid tumors. *Proc Natl Acad Sci U S A*. 2012;109(17):6662–6667.
10. Majeti R, et al. CD47 is an adverse prognostic factor and therapeutic antibody target on human acute myeloid leukemia stem cells. *Cell*. 2009;138(2):286–299.
11. Liu J, et al. Pre-clinical development of a humanized anti-CD47 antibody with anti-cancer therapeutic potential. *PLoS One*. 2015;10(9):e0137345.
12. Jaiswal S, et al. CD47 is upregulated on circulating hematopoietic stem cells and leukemia cells to avoid phagocytosis. *Cell*. 2009;138(2):271–285.
13. Chao MP, et al. Anti-CD47 antibody synergizes with rituximab to promote phagocytosis and eradicate non-Hodgkin lymphoma. *Cell*. 2010;142(5):699–713.
14. Kim D, Wang J, Willingham SB, Martin R, Wernig G, Weissman IL. Anti-CD47 antibodies promote phagocytosis and inhibit the growth of human myeloma cells. *Leukemia*. 2012;26(12):2538–2545.
15. Advani R, et al. CD47 blockade by Hu5F9-G4 and rituximab in non-Hodgkin's lymphoma. *N Engl J Med*. 2018;379(18):1711–1721.
16. Tsai RK, Discher DE. Inhibition of "self" engulfment through deactivation of myosin-II at the phagocytic synapse between human cells. *J Cell Biol*. 2008;180(5):989–1003.
17. Timms JF, et al. Identification of major binding proteins and substrates for the SH2-containing protein tyrosine phosphatase SHP-1 in macrophages. *Mol Cell Biol*. 1998;18(7):3838–3850.

18. Kharitonenkov A, Chen Z, Sures I, Wang H, Schilling J, Ullrich A. A family of proteins that inhibit signalling through tyrosine kinase receptors. *Nature*. 1997;386(6621):181–186.
19. Fujioka Y, et al. A novel membrane glycoprotein, SHPS-1, that binds the SH2-domain-containing protein tyrosine phosphatase SHP-2 in response to mitogens and cell adhesion. *Mol Cell Biol*. 1996;16(12):6887–6899.
20. Adams S, et al. Signal-regulatory protein is selectively expressed by myeloid and neuronal cells. *J Immunol*. 1998;161(4):1853–1859.
21. Queen C, et al. A humanized antibody that binds to the interleukin 2 receptor. *Proc Natl Acad Sci U S A*. 1989;86(24):10029–10033.
22. Carter PJ. Potent antibody therapeutics by design. *Nat Rev Immunol*. 2006;6(5):343–357.
23. Ring NG, et al. Anti-SIRPα antibody immunotherapy enhances neutrophil and macrophage antitumor activity. *Proc Natl Acad Sci U S A*. 2017;114(49):E10578–E10585.
24. Takenaka K, et al. Polymorphism in Sirpa modulates engraftment of human hematopoietic stem cells. *Nat Immunol*. 2007;8(12):1313–1323.
25. Sim J, et al. Discovery of high affinity, pan-allelic, and pan-mammalian reactive antibodies against the myeloid checkpoint receptor SIRPα. *MAbs*. 2019;11(6):1036–1052.
26. Barclay AN, Brown MH. The SIRP family of receptors and immune regulation. *Nat Rev Immunol*. 2006;6(6):457–464.
27. Piccio L, et al. Adhesion of human T cells to antigen-presenting cells through SIRPbeta2-CD47 interaction costimulates T-cell proliferation. *Blood*. 2005;105(6):2421–2427.
28. Brooke G, Holbrook JD, Brown MH, Barclay AN. Human lymphocytes interact directly with CD47 through a novel member of the signal regulatory protein (SIRP) family. *J Immunol*. 2004;173(4):2562–2570.
29. Sikic BI, et al. First-in-human, first-in-class phase I trial of the anti-CD47 antibody Hu5F9-G4 in patients with advanced cancers. *J Clin Oncol*. 2019;37(12):946–953.
30. Ritchie M, Tchistiakova L, Scott N. Implications of receptor-mediated endocytosis and intracellular trafficking dynamics in the development of antibody drug conjugates. *MAbs*. 2013;5(1):13–21.
31. Panowski S, Bhakta S, Raab H, Polakis P, Junutula JR. Site-specific antibody drug conjugates for cancer therapy. *MAbs*. 2014;6(1):34–45.
32. Nath N, et al. Homogeneous plate based antibody internalization assay using pH sensor fluorescent dye. *J Immunol Methods*. 2016;431:11–21.
33. Casi G, Neri D. Antibody-drug conjugates: basic concepts, examples and future perspectives. *J Control Release*. 2012;161(2):422–428.
34. Lammerts van Bueren JJ, et al. Effect of target dynamics on pharmacokinetics of a novel therapeutic antibody against the epidermal growth factor receptor: implications for the mechanisms of action. *Cancer Res*. 2006;66(15):7630–7638.
35. Chaparro-Riggers J, et al. Increasing serum half-life and extending cholesterol lowering in vivo by engineering antibody with pH-sensitive binding to PCSK9. *J Biol Chem*. 2012;287(14):11090–11097.
36. Amano J, et al. Antigen-dependent internalization is related to rapid elimination from plasma of humanized anti-HM1.24 monoclonal antibody. *Drug Metab Dispos*. 2010;38(12):2339–2346.
37. van Beek EM, Cochrane F, Barclay AN, van den Berg TK. Signal regulatory proteins in the immune system. *J Immunol*. 2005;175(12):7781–7787.